

Supplemental information

Box size limitations

It is important to note that finite size effects likely play a role in the resultant structure formed by the micelles. Ideally, the system should be large enough that an addition or removal of a micelle does not significantly affect the structure formed. The small size of the simulation box also prevents the observation of any meaningful ordered structures in the flow-vorticity or flow-gradient micelle planes (3D structures). Generally, each plane contains only two or three micelles, making the extrapolated structures trivial. Addressing this problem requires either a larger-scale simulation approach or the exploitation of high performance computing resources using the current methods.

A study was done where the simulation box size was doubled in all dimensions to determine how the dynamics would be affected by the smaller simulation box. The streamlines are shown for two similarly sized micelles in Fig. S1. The key features are seen in both systems: the rotational flow field, the inclination of the micelles, and stagnation points. The primary difference between the two systems is that the stagnation points in the large system are discrete, whereas in the small system they straddle a periodic boundary, and therefore are same point. A3B6 polymers were also used to determine whether they would make a good alternative to using very large systems, by decreasing the micelle size. The streamlines and vorticity contour plots for these data are shown in Fig. S2. Although the stagnation points are discrete in the small polymer system (A3B6), the inclination angle and the flow-deviation field shown significant differences as compared to the longer polymer systems.

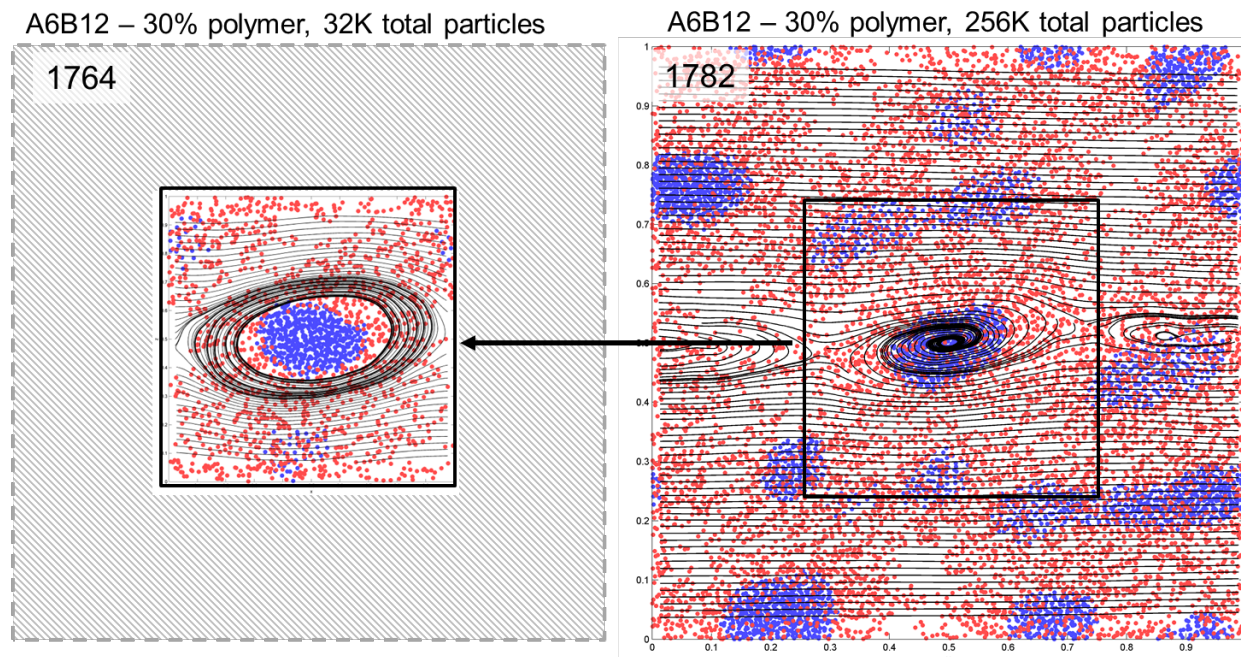


Fig S1. Size comparison between the 256K particle simulation (right) and the normal 32K particle simulation (left). Important in this comparison is the two distinct flow stagnation points visible in the larger 256K simulation, but not in the 32K particle simulation. In the smaller box, the stagnation points lie on the periodic boundary in the flow direction, effectively forming a single stagnation point.

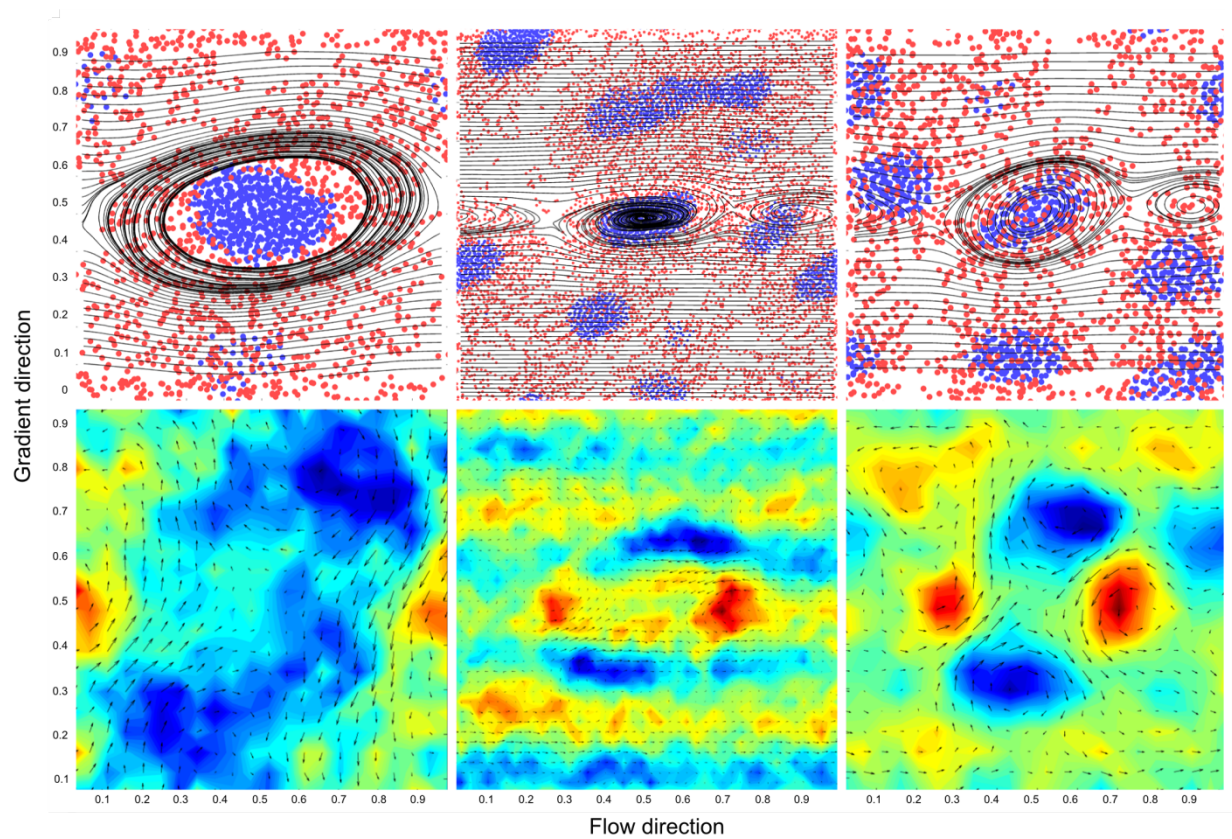


Fig S2. Flow behaviour relative to several example micelles from different systems. Top row shows approximate streamlines for all particle motion. Bottom row shows deviations from a linear profile (vector field) and angular velocity (contour s). An A6-B12 micelle (1782 particles) in the 32K particle system used throughout this paper (left column) and a larger one (2682 particles) from a 256K particle system. Also shown (right column) are results from a A3B6 system. 30% polymer, $\dot{\gamma} = 0.002\tau^{-1}$.

Kinetically Trapped Micelles

As mentioned in the paper, the micelles are believed to be kinetically trapped in the quiescent state. This is evident in the difference in cluster distributions seen in Figure S3 for all four different polymer lengths (A6B12, A6B9, A6B6, and A6B3). In all cases, the average size of micelles increases and the number of micelles decrease. Only in the shortest hydrophilic block simulation are the differences between the unsheared and sheared systems small. The resulting sheared micelles for each polymer system have been collected and shown in Figure S4. As seen in the aforementioned cluster histograms, there is a larger disparity in micelle sizes with the shorter hydrophilic block length systems. This disparity is also evident in the snapshots of Figure S4, where elongated micelles are seen for

every system except for the A6B12 system.

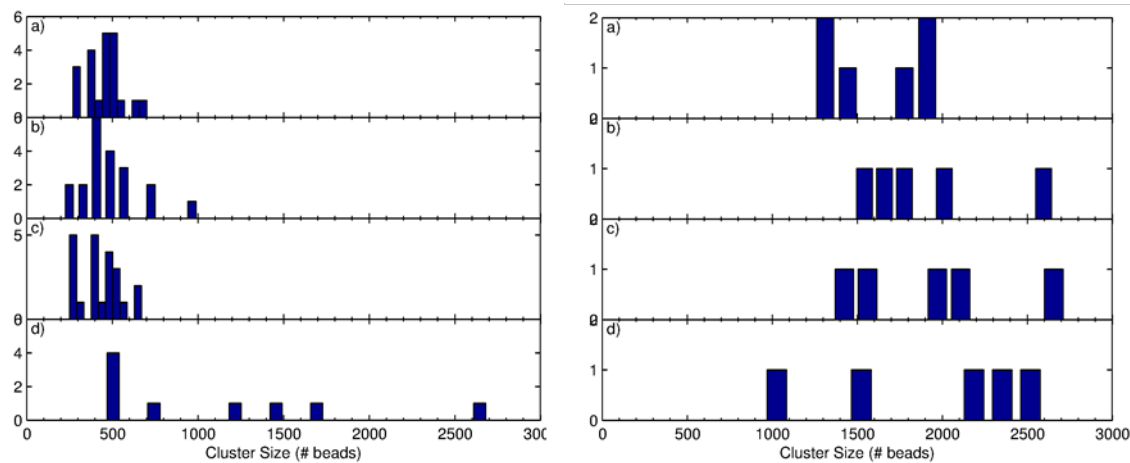


Fig S3. Cluster size distributions – (Left) Distributions of clusters after 2,000,000 non-sheared MD steps from a random state for (a) A6B12, (b) A6B9, (c) A6B6 and (d) A6B3. Notice the similarities between corona lengths 12 through 6, but the sharp change in distribution with the shortest corona length. (Right) After 2,000,000 sheared MD steps at $\dot{\gamma} = 0.002\tau^{-1}$ (A6B12 is after 3,000,000 steps) clusters undergo fusion, forming fewer, larger clusters.

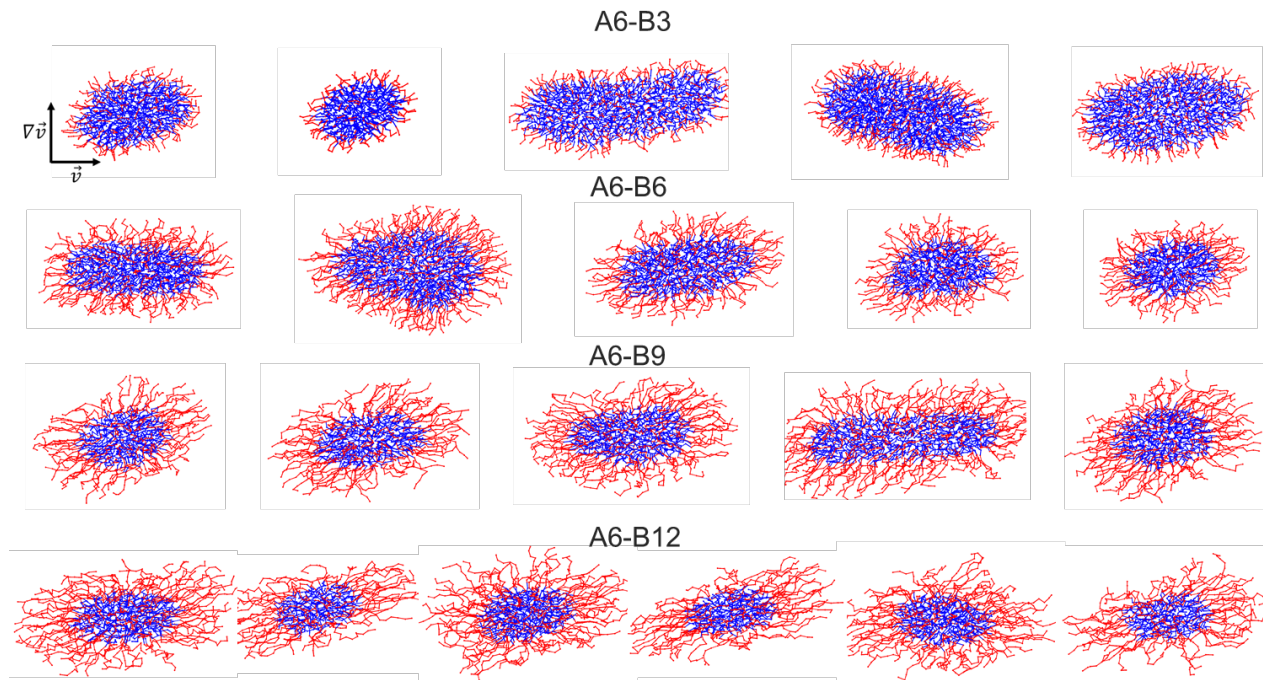


Fig S4. Gradient-flow views of clusters formed after 2,000,000 sheared MD steps at $\dot{\gamma} = 0.002\tau^{-1}$ for the four corona lengths tested..

Elongated micelles can be seen in the A6B3, A6B6 and A6B9 systems. In contrast, the A6B12 system is comprised only of spherical micelles.

Shear Rheology

The shear rheology of the polymers used in these simulations was explored within the range of the shear ordering results ($0.001\tau^{-1} - 0.01\tau^{-1}$). In this range, we see shear thinning behaviour for all the polymers tested as should be expected. These results are shown with error bars in Figure S5. Note, the error bars are large at low shear rates because the shear viscosity is calculated with $\eta = -P_{xz}/\dot{\gamma}$ and noise in the P_{xz} data at low shear rates tends to be large. The shear viscosity for each polymer system at $\dot{\gamma} = 0.002\tau^{-1}$ are shown in Figure S6, showing a weak dependence on the corona length. The shortest corona length system does indeed exhibit a decreased viscosity beyond the bounds of the error bars. At present, it is unclear to the authors whether this is a result of a change in the micelle sizes/morphology, or a direct result of the decreased hydrophilic block length.

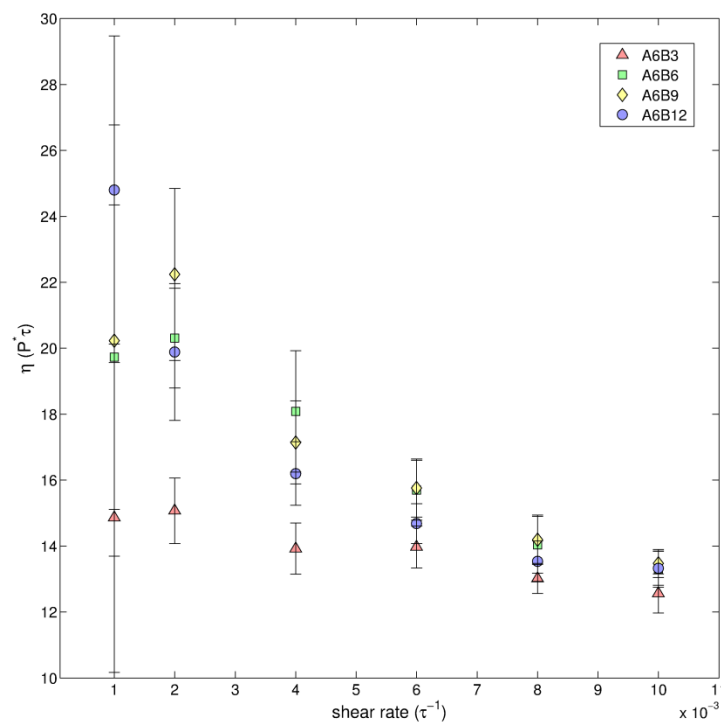


Fig S5. Shear viscosity as a function of the corona length for the four corona-length systems as a function of shear rate. Error bars are determined from the standard deviation of the instantaneous viscosity over the sampling period.

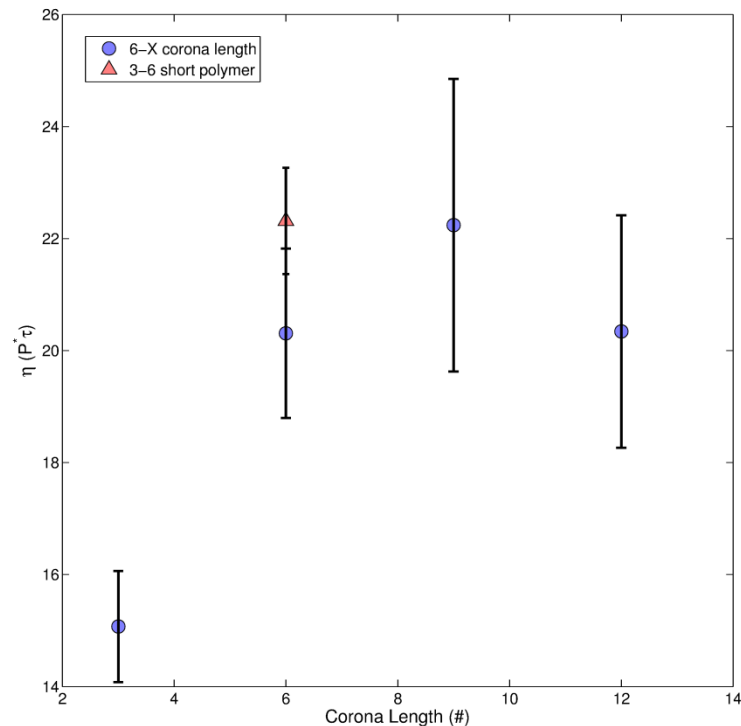


Fig S6. Shear viscosity as a function of the corona length for the four systems studied at $\dot{\gamma} = 0.002\tau^{-1}$ (data from Fig. S6). The viscosity of the A3B6 polymer is also plotted for reference. Error bars are determined from the standard deviation of the instantaneous viscosity over the sampling period.

We have also examined the shear viscosity at $\dot{\gamma} = 0.002\tau^{-1}$ for the A6B12 system as a function of polymer concentration (shown in Figure S7). As the concentration of the polymer increases, the shear viscosity also increases as expected. The increase in polymer concentration corresponds to a change in the micelle morphology, eventually forming cylinders when the shear viscosity is greatest. When the system becomes a melt, there is a drop in the viscosity as is expected when all the solvent has been removed.

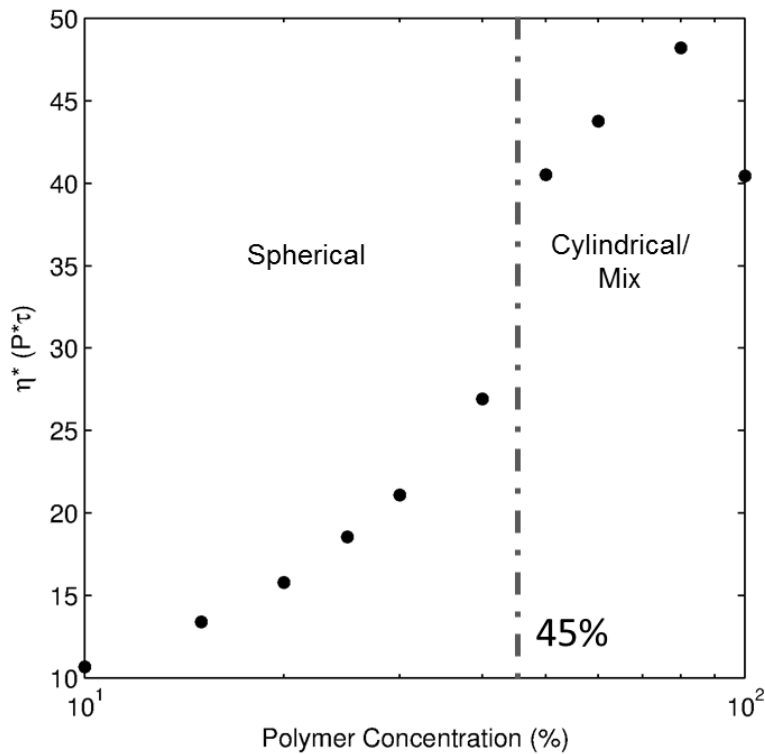


Fig S7. Shear viscosity as a function of concentration for the A6-B12 30wt% system at $\dot{\gamma} = 0.002\tau^{-1}$.

Nanoparticle Diffusion

The Stokes-Einstein relationship ($D = k_B T / 6\pi\eta r$) has been verified for the point-type (colloid potential) particles used in our simulations and these results are shown in Figure S8. These simulations were performed using single nanoparticles in a solvent bath of 4000 particles. The position of the minimum in the colloid potential was used to define the particle radius r .

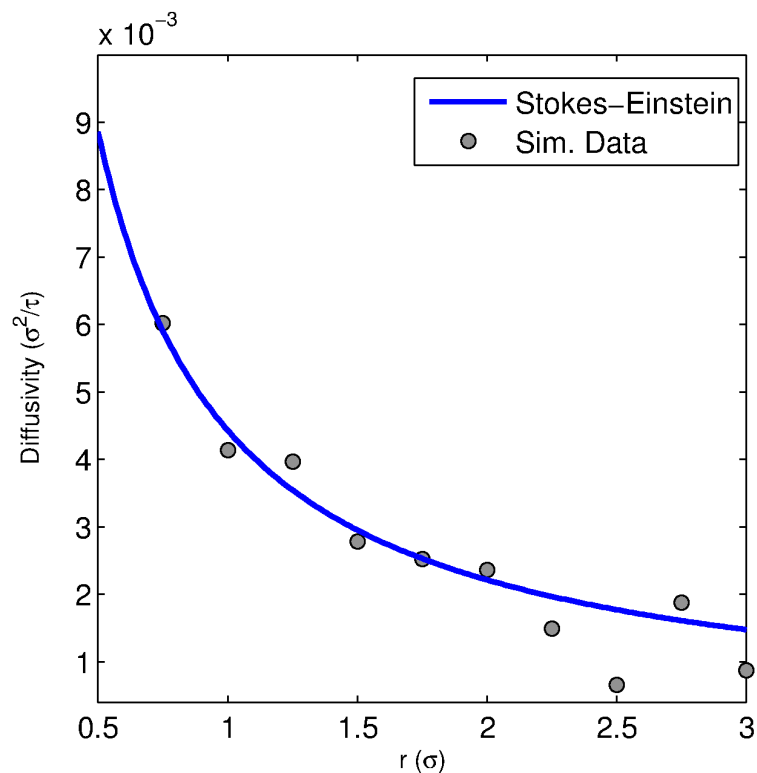


Fig S8. Measured diffusivity of nanoparticles as a function of their radius (circles) compared against the Stokes-Einstein prediction (solid line) for the solvent used in these simulations.

Micelle Rotation

The rotational frequency of the micelles in all systems was calculated by tracking particles at the corona/core boundary and averaging their angular displacement over duration of 500,000 time steps. There is a little correlation between corona length and rotational frequency, but a clear decreasing trend with increasing micelle size. This behaviour is a result of the increased core/corona surface area (and circumference in 2D) with a constant surface velocity.

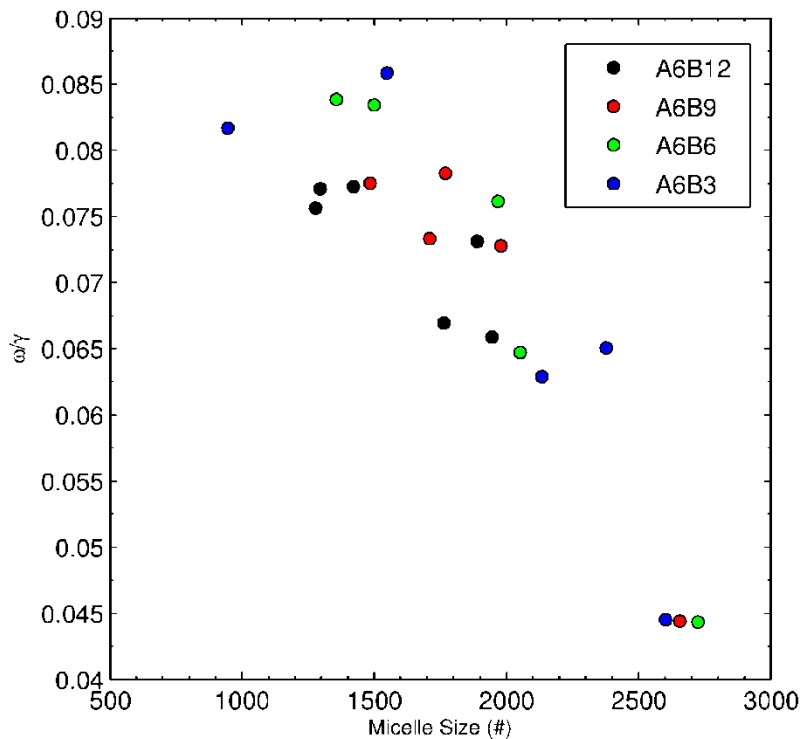


Fig S9. Shown are the dimensionless rotational frequencies ($\omega/\dot{\gamma}$) for the micelles found in each system plotted against their size (particle number).